Published in final edited form as:
J Phys Chem B. 2013 August 1; 117(30): 8994–9003. doi:10.1021/jp402394m.

Formation of Cholesterol Bilayer Domains Precedes Formation of Cholesterol Crystals in Cholesterol/ Dimyristoylphosphatidylcholine Membranes: EPR and DSC Studies

Laxman Mainali[a], **Marija Raguz**[a,b], and **Witold K. Subczynski**[a,*]

[a]Department of Biophysics, Medical College of Wisconsin, Milwaukee, Wisconsin 53226, USA

[b]Department of Medical Physics and Biophysics, School of Medicine, University of Split, Split, Croatia

Abstract

Saturation-recovery EPR along with DSC were used to determine the cholesterol content at which pure cholesterol bilayer domains (CBDs) and cholesterol crystals begin to form in dimyristoylphosphatidylcholine (DMPC) membranes. To preserve compositional homogeneity throughout the membrane suspension, lipid multilamellar dispersions were prepared using a rapid solvent exchange method. The cholesterol content increased from 0 to 75 mol%. With spin-labeled cholesterol analogs it was shown that the CBDs begin to form at ~50 mol% cholesterol. It was confirmed by DSC that the cholesterol solubility threshold for DMPC membranes is detected at ~66 mol% cholesterol. At levels above this cholesterol content, monohydrate cholesterol crystals start to form. The major finding is that formation of CBDs precedes formation of cholesterol crystals. The region of the phase diagram for cholesterol contents between 50 and 66 mol% is described as a structured one-phase region in which CBDs have to be supported by the surrounding DMPC bilayer saturated with cholesterol. Thus, the phase boundary located at 66 mol % cholesterol separates the structured one-phase region (liquid-ordered phase of DMPC with CBDs) from the two-phase region where the structured liquid-ordered phase of DMPC coexists with cholesterol crystals. It is likely that CBDs are precursors of monohydrate cholesterol crystals.

Keywords

cholesterol; cholesterol bilayer domain; cholesterol crystals; membrane; spin label; EPR

INTRODUCTION

Differential scanning calorimetry (DSC) [1–4], X-ray diffraction [1,2,5–8], and the MAS NMR [3,9] have been used to identify and characterize the structure of immiscible cholesterol (Chol) aggregates (or domains) formed in model and biological membranes at an elevated Chol content. In their review paper, Bach and Wachtel [10] discuss the application of these methods in detection of Chol crystals. However, Mason and co-authors [5,11] indicate in their reviews that these techniques also confirm formation of Chol crystalline domains that are precursors of Chol crystals. These Chol domains have often been depicted as pure Chol bilayers surrounded by the bulk phospholipid (PL) bilayer containing Chol [5,7,8,11–18], and in

*CORRESPONDING AUTHOR: Witold K. Subczynski, Ph.D., Department of Biophysics, Medical College of Wisconsin, 8701 Watertown Plank Road, Milwaukee, WI 53226, USA, Tel: (414) 955-4038, Fax: (414) 955-6512, subczyn@mcw.edu.

the literature they have often been called *cholesterol crystalline domains*, *cholesterol crystallites*, or, simply, *cholesterol crystals*. It was also assumed that Chol crystalline domains should possess the same bulk properties as those found in one of three previously characterized triclinic Chol crystals (formed without phospholipids) [19]. These properties include (1) the polymorphic phase transition of the anhydrous form of Chol observed at 36°C and the dehydration of the monohydrate form observed at 76°C using DSC; (2) the characteristic diffraction peaks of 34 Å observed by small-angle X-ray diffraction; and (3) the rigid structure of the domain. However, results obtained from these techniques do not explain why the pure Chol bilayer possesses the same properties as rigid Chol crystals. Specifically, (1) the accessibility of water to Chol –OH groups is not limited in the hydrated bilayer, and the presence of the anhydrous form of Chol shown by phase transitions seems unlikely. Additionally, models created with molecular dynamics simulations showed that, on average, each Chol molecule in the pure Chol bilayer makes 2.3 hydrogen bonds with water, as compared with 1.7 hydrogen bonds in the PL-Chol bilayer (the maximum average number of hydrogen bonds per Chol is 3) [20]. (2) Spacing of 34 Å observed by small-angle X-ray diffraction would require the presence of multiple layers of Chol, which is equivalent to three-dimensional (crystal) structures and not to the two-dimensional Chol bilayer. A single Chol bilayer immersed in the membrane plane would not produce the small-angle repeat period. Bach and Wachtel [10] have previously shown that the necessary prerequisite to detect 34 Å peaks using small-angle X-ray diffraction is a sufficiently large number of Chol pseudo bilayers in the crystallites (thus, a three-dimensional structure is necessary). (3) None of the techniques mentioned above attempted to, or were able to, provide information about the dynamics of Chol molecules in the domains.

We use electron paramagnetic resonance (EPR) spin-labeling methods extensively to study the organization and dynamics of PL membranes with high Chol contents [21–24]. These methods provide missing information on the organization and dynamics of Chol molecules in the Chol domains. These studies indicate that Chol molecules in this domain form a bilayer-like structure with order and rotational motion of Chol molecules similar to those in the surrounding PL bilayer saturated with Chol [22,24], and different from the rigid structure of Chol crystals discriminated by the X-ray diffraction and DSC [1–3,5,6,8]. Therefore, we have named domains that have been discriminated and characterized by the EPR spin-labeling method *cholesterol bilayer domains* (CBDs) to indicate their (dynamic) bilayer structure and difference from the (rigid) crystalline structure. The CBD is formed only in the presence of PLs and cannot exist as a free bilayer in the buffer [21]. Our earlier results [21–24] showed that the CBD was present in all investigated membrane suspensions when the mixing ratio exceeded the Chol solubility threshold (CST). Also investigations done through the molecular dynamics (MD) simulations confirmed that the CBD is a dynamic structure with Chol mobility similar to that in membranes saturated with Chol [20,25].

In our earlier papers [21–24] and in most other papers, the formation of CBDs, Chol crystalline domains, Chol crystallites, or Chol crystals were investigated in membranes prepared using the film deposition method. The only explanation of our earlier results that did not contradict other well-documented data from literature, was that when the Chol content in the PL bilayer exceeds the CST, both the CBD and Chol crystals form in the membrane suspension. The former was detected by EPR spin-labeling methods, the latter by DSC as well as the X-ray diffraction. The warning came from the critical evaluation of the film deposition method of membrane preparation [26,27]. It was indicated that during membrane preparations using the film deposition method, the lipid mixture passed through the solid state intermediate at which solid-state demixing of Chol can occur, producing falsely low estimates of the CST. Phosphatidylcholine (PC) liposomes prepared using the film deposition method showed the CST at a Chol/PC molar ratio of 1 [26,28] while those prepared using the rapid solvent exchange method showed the CST at a Chol/PC molar ratio of 2 [26]. It indicates that Chol

molecules that are trapped in Chol crystals during membrane preparation using the film deposition method do not participate in further liposome formation. Additionally, at Chol contents greater than the CST, both anhydrous and monohydrate Chol crystals were formed during film deposition liposome preparations [3,26,28], and only monohydrate Chol crystals were formed during rapid solvent exchange preparations [26]. Thus, obtaining the missing information about the organization of lipids for Chol content between the false and the true CST is a timely task, and was the major goal of this research.

We present results of discrimination of the CBD (using EPR spin-labeling) and Chol crystals (using DSC) in dimyristoylphosphatidylcholine (DMPC) liposomes prepared using the rapid solvent exchange method. Thanks to this method of liposome preparation, we were able to show that the formation of CBDs precedes formation of cholesterol crystals. CBDs are formed for the Chol content equal to or exceeding the Chol/DMPC molar ratio of ~1 (50 mol% Chol). Using DSC, we also confirmed results obtained earlier by X-ray diffraction for other PCs [26], that Chol crystals are formed only when the Chol content is equal to or exceeds the Chol/DMPC molar ratio of ~2 (66 mol% Chol). We chose the Chol/DMPC membranes to demonstrate these new results because properties for this system are readily available in the literature, and the phase diagram is well established [29]. Figure 1 indicates temperature and Chol/DMPC mixing ratios at which experiments were performed, and is used as a guideline for the presentation of our data. Experiments were performed for Chol contents extending beyond the established phase diagram (included in Fig. 1) to the region where DMPC membranes are saturated and oversaturated with Chol. Figure 1 also contains schematic drawings of the organization of lipid molecules in purported phases and domains that, we expect, should exist at certain Chol contents.

EXPERIMENTAL METHODS

Preparation of membrane suspensions using rapid solvent exchange method

The membranes used in this study were multilameller dispersions of DMPC and Chol (Avanti Polar Lipids, Alabaster, AL) prepared using the rapid solvent exchange method [26,27,30] with the apparatus that was built as described in details in [30]. This improved design increased solvent-removal efficiency twofold. Chloroform solutions of lipids were mixed to attain a desired Chol/DMPC mixing ratio from 0 to 3. Chloroform solutions with a final volume of 75 μL to 200 μL were added at 27°C to the 1.2 mL of buffer (10 mM PIPES and 150 mM NaCl, pH 7.0) in a test tube. As described [30], the tube was mounted on a laboratory vortexer and coupled to the sample manifold of the rapid solvent exchange device. The vortexer was actuated, the flushing-argon flow rate was confirmed, and the manifold valve was quickly opened to a trap-protected vacuum system preset at ~25 torr. After the appropriate time elapsed, the vortexer was stopped, the manifold was vented, and the sample tube was removed from the device. To ensure that all chloroform was removed, samples were kept under the reduced pressure for four minutes, which caused reduction of the buffer volume to 1.0 mL. The membrane suspensions were then used for EPR and DSC experiments.

For EPR measurements, all samples contained 0.5×10^{-5} mol of total lipids with 1 mol% of Chol analog spin labels, the androstane spin label (ASL), or the cholestane spin label (CSL) (Molecular Probes, Eugene, OR. See Fig. 2 for their structures). For DSC measurements, all samples contained the same amount of Chol (14 mg/mL) and appropriately adjusted concentration of DMPC.

Saturation-recovery EPR measurements

Membrane suspensions were centrifuged briefly, and the loose pellet (~20% lipid, wt/wt) was used for saturation-recovery (SR) EPR measurements (using an SR EPR X-band

spectrometer equipped with a loop-gap resonator [31]). The sample was placed in a 0.6 mm i.d. capillary made of a gas-permeable methylpentene polymer called TPX [32]. Spin-lattice relaxation times (T_1s) were determined by analyzing the SR signal of the central line obtained in short pulse experiments [31]. For measurements of the oxygen transport parameter (see section below), the sample was equilibrated with the same gas that was used for temperature control [*i.e.,* a controlled mixture of nitrogen and dry air adjusted with flow meters (Matheson Gas Products, model 7631H-604)] [33,34]. For measurements of the NiEDDA accessibility parameter (see section below), a 20 mM NiEDDA was present in the buffer [21,22]. All EPR measurements were performed at 27°C. Typically, 10^5 –10^6 decays were acquired with 2048 data points on each decay. Sampling intervals 2, 2.5, 4, 5, 10, or 20 ns were used for measurements. The total accumulation time was typically 2–5 min. SR signals were fitted by single- or double-exponential functions. When a single-exponential fit was satisfactory, the standard deviation of the decay time constants for independent experiments (for samples prepared totally independently) was within 3% of the mean. When a double-exponential fit was necessary, and satisfactory, the decay times were usually evaluated with standard deviations less than ±5% and ±10% for longer and shorter recovery time constants, respectively.

Oxygen transport parameter and NiEDDA accessibility parameter

Relaxation agents, molecular oxygen, and NiEDDA induce spin exchange, which lead to faster spin-lattice relaxation of the nitroxide. The rate of bimolecular collisions between either molecular oxygen or NiEDDA and the nitroxide moiety of a spin label placed at a specific location in the membrane is evaluated from the T_1s of the spin label.

The oxygen transport parameter, W(x), was introduced as a convenient quantitative measurement of the collision rate between spin label and molecular oxygen [33]:

$$W(x)=T_1^{-1}(\mathrm{Air},x)-T_1^{-1}(N_2,x)\sim D(x)C(x), \quad (1)$$

where W(x) is normalized to the sample equilibrated with air at normal pressure and is proportional to the product of the translational diffusion coefficient, D(x), and the concentration, C(x), of oxygen at a depth “x” in the membrane.

Similarly, the accessibility parameter, P(x), for the water-soluble, neutral relaxation agent NiEDDA was defined as [21,22]:

$$P(x)=T_1^{-1}(20\,\mathrm{mM\ NiEDDA},x)-T_1^{-1}(\mathrm{NO\ NiEDDA},x). \quad (2)$$

Greater P(x) values indicate a greater extent of NiEDDA penetration into the membrane. All accessibility measurements must be performed for deoxygenated samples.

DSC measurements

Measurements of DSC were made using a Nano DSC with Platinum capillary cells obtained from TA instruments. The capillary cell has a volume of 0.3 mL. The Nano DSCRun operating system software was used to acquire data, and NanoAnalyze data analysis software was used for data analysis. A constant scan rate of 1°C/min was used. The heat of transition was evaluated with a standard deviation smaller than ±25% from the mean value for independent experiments (for samples prepared independently).

RESULTS

Cholesterol-analog spin labels interact differently with membrane-soluble and water-soluble relaxation agents

Chol analog spin labels (ASL and CSL) were used. These spin labels have molecular structures similar to parent Chol (Fig. 2) and, therefore, are expected to behave and similarly distribute across different membrane domains. In our previous paper [21] and in the present research (see the section, "CBDs form at cholesterol content lower than the CST"), we confirmed that the distribution of Chol analog spin labels between the CBD and the surrounding PL membrane saturated with Chol is close to the expected distribution of Chol.

SR signals of ASL (sensitivity to hydrophobic and polar relaxation agents)— Figures 3A and B show representative saturation-recovery signals for ASL in Chol/DMPC membranes with a mixing ratio of 1.5, at 27°C, in the presence and absence of the hydrophobic relaxation agent, oxygen (Fig. 3A), and in the presence and absence of the water soluble, neutral relaxation agent, NiEDDA (Fig. 3B). This Chol content is lower than the CST in PC membranes prepared using the rapid solvent exchange method, observed at Chol/PC mixing ratio of 2 [26]. DMPC liposomes for all investigations were prepared using the rapid solvent exchange method. SR signals were fitted using single- and double-exponentials and compared. The single-exponential fit was satisfactory for ASL in deoxygenated membranes (top residuals, Figs. 3A and B). For ASL in the presence of oxygen, the single-exponential fit was not satisfactory (middle residual, Fig. 3A), while the double-exponential fit was excellent (bottom residual, Fig. 3A). These results indicate that, under these conditions, ASL is located in two environments (two domains) in which the collision rate of molecular oxygen with the nitroxide moiety of ASL is quite different. Thus, using the discrimination by oxygen transport method and ASL, the existence of two domains can be confirmed. Assignment of these data to appropriate domains (to the bulk DMPC bilayer saturated with Chol and to the CBD) is only possible when the oxygen transport parameter values are calculated (Fig. 4A). [21–23]

All SR signals obtained with ASL for membranes in the presence of NiEDDA were single-exponentials (bottom residual, Fig. 3B). Based on similarities of SR curves presented in Fig. 3B, we concluded that in both the bulk DMPC bilayer saturated with Chol and in the CBD, NiEDDA does not penetrate to the depth at which the nitroxide moiety of ASL is located. These results are in agreement with hydrophobicity measurements around the nitroxide moiety of ASL [22,23]. We confirmed earlier for various PL membranes that, independent of Chol content, the more polar –OH group of ASL is always located in the headgroup region and the less polar nitroxide moiety is located in the hydrocarbon-chain region, close to the membrane center [22,23]. We also confirmed this result for the Chol/DMPC membrane (data not shown).

SR signals of CSL (sensitivity to hydrophobic and polar relaxation agents)— Figures 3C and D show representative saturation-recovery signals for CSL in Chol/DMPC membranes with a mixing ratio of 1.5, at 27°C, in the presence and absence of oxygen (Fig. 3C) and in the presence and absence of NiEDDA (Fig. 3D). The single-exponential fit was satisfactory for CSL in deoxygenated membranes (top residuals, Figs. 3C and D). Measurements with CSL show that in the presence of NiEDDA, a single-exponential fit was not satisfactory (middle residual, Fig. 3D), while the double-exponential fit was excellent (bottom residual, Fig. 3D). These results indicate that under these conditions, CSL is located in two environments (two domains) in which the collision rate of NiEDDA with the nitroxide moiety of CSL is quite different. Thus, the existence of two domains can also be confirmed with CSL and NiEDDA as a relaxation agent. Assignment of these data to

appropriate domains (to the bulk DMPC bilayer saturated with Chol and to the CBD) is only possible when the NiEDDA accessibility parameter values are calculated (Fig. 4B). [21–23]

All SR signals obtained with CSL for membranes in the presence of oxygen were single-exponentials (bottom residual, Fig. 3C). Because (as we showed above) CSL is distributed between the bulk DMPC bilayer saturated with Chol and the CBD, we concluded that the collision rate between oxygen and the nitroxide moiety of CSL is the same in these (see also the section below and the discussion in Ref. [35]).

Discrimination of the CBD by cholesterol-analog spin labels

Our discrimination method [36] is a dual-probe SR EPR approach in which the observable parameter is the T_1 of spin labels, and the measured values is the bimolecular collision rate between the nitroxide moiety of spin labels and relaxation agent [molecular oxygen, or water soluble NiEDDA, see Eqs. (1) and (2)]. When located in two different membrane domains, the spin label alone often cannot differentiate between these domains, giving very similar (indistinguishable) conventional EPR spectra and similar T_1 values. This is the case for Chol analog spin labels in the CBD and the surrounding PL bilayer with similar order parameter (similar conventional EPR spectra) and similar motion (similar T_1s) [21–23]. However, even small differences in lipid packing in these domains will affect solubility (partitioning) and translational diffusion of molecular oxygen and NiEDDA, which can be easily detected by observing the different T_1s from spin labels in these two locations in the presence of relaxation agents. Our approach indicates differences in the bulk properties of the CBD and surrounding DMPC bilayer saturated with Chol (DMPC-Chol), namely, differences in solubility (partitioning) and in translational diffusion coefficient of molecular oxygen or NiEDDA).

The oxygen transport parameter, W(x), in the CBD and in the surrounding DMPC-Chol bilayer can be calculated based on T_1 values obtained from double-exponential fits for samples equilibrated with air and from single-exponential fits for samples equilibrated with nitrogen (as in Fig. 3A):

$$W(\mathrm{CBD}) = T_1^{-1}(\mathrm{Air},\ \mathrm{CBD}) - T_1^{-1}(N_2, \mathrm{CBD}), \quad (3)$$

$$W(\mathrm{DMPC{-}Chol}) = T_1^{-1}(\mathrm{Air},\ \mathrm{DMPC{-}Chol}) - T_1^{-1}(N_2,\ \mathrm{DMPC{-}Chol}). \quad (4)$$

In our samples T_1 (N_2, CBD) = T_1 (N_2, DMPC-Chol).

The NiEDDA accessibility parameter, P(x), in the CBD and in the surrounding DMPC-Chol bilayer can be calculated based on T_1 values obtained from double-exponential fits for samples in the presence of 20 mM NiEDDA in the buffer, and from single-exponential fits for samples without NiEDDA (equilibrated with nitrogen) (as in Fig. 3D):

$$P(\mathrm{CBD}) = T_1^{-1}(20\,\mathrm{mM\ NiEDDA},\ \mathrm{CBD}) - T_1^{-1}(\mathrm{No\ NiEDDA},\ \mathrm{CBD}), \quad (5)$$

$$P(\mathrm{DMPC{-}Chol}) = T_1^{-1}(20\,\mathrm{mM\ NiEDDA},\ \mathrm{DMPC{-}Chol}) - T_1^{-1}(\mathrm{No\ NiEDDA},\ \mathrm{DMPC{-}Chol}). \quad (6)$$

In our samples T_1 (No NiEDDA, CBD) = T_1 (No NiEDDA, PL-Chol).

Discrimination by oxygen transport—The discrimination by oxygen transport method (see Eqs. 1, 3, and 4) was applied for membranes with a Chol/DMPC mixing ratio between 0 and 3, for mixing ratios lower and greater than the CST. The final results for these measurements are presented in Figure 4A. We were able to detect two domains when the Chol/DMPC mixing ratio was greater than 1. Measurements of the oxygen transport parameter performed for a wide range of Chol content allowed assignment of SR results which give the greater oxygen transport parameter to the bulk DMPC bilayer saturated with Chol (DMPC-Chol) and the remaining SR results to the CBD. Results presented in Figure 4A confirmed that the CBD can be detected for Chol content lower than the CST in the DMPC bilayer.

Values of the oxygen transport parameter assigned to the DMPC-Chol (including that one obtained at the Chol/DMPC molar ratio of 1) are the same as in the DMPC membrane containing 50 mol% Chol and obtained with the 10-PC spin label [37]. We should note that nitroxide moieties of ASL and 10-PC are located at the same depth in lipid bilayer membranes. Additionally, n-PC spin labels do not partition into the CBD giving profiles of the oxygen transport parameter across the DMPC-Chol without “contaminations” from the CBD [21–23,35]. Values of the oxygen transport parameter in the CBD are also close to those obtained earlier for CBDs in lens lipid membranes [35,38–40] and in simple model membranes [21–23]. All these additionally confirm our assignment. Results presented in Figure 4A indicate that the oxygen transport parameter in the center of the CBD (at the position of the nitroxide moiety of ASL) is about 2.5 to 5 times smaller than in the center of the bulk DMPC-Chol. Although the CSL data (Fig. 4A) show a single value for the oxygen transport parameter for all Chol contents, indicating that the collision rate between the nitroxide moiety of CSL and oxygen in both domains is the same and CSL, which is located in both domains, cannot discriminate between them. In the presented research we did not pay attention to coexisting liquid-disordered and liquid-ordered phases for Chol/DMPC mixing ratio lower than 1/2. These data were already published [37].

Discrimination by water soluble relaxation agent accessibility—The final results of SR measurements with NiEDDA are presented in Figure 4B showing that CSL is located in both the bulk DMPC-Chol and the CBD, and that these domains can be discriminated using the NiEDDA accessibility parameter (see Eqs. 2, 5, and 6). We were able to detect two domains when the Chol/DMPC mixing ratio was greater than 1, confirming results obtained using the discrimination by oxygen transport method. The nitroxide moiety of CSL is more exposed to collisions with water soluble NiEDDA when it is located in the CBD, and its nitroxide moiety is not protected by the “umbrella” effect of PL headgroups (as in the bulk DMPC bilayer saturated with Chol). However, the umbrella model cannot explain formation of the CBD. This model suggests that in a bilayer, Chol relies on the coverage by the large polar headgroups of the neighboring PLs to prevent the unfavorable free energy of exposure of the nonpolar part of Chol to water [41,42]. The accessibility of the water soluble relaxation agent to Chol in the CBD is a few times greater than to Chol in the surrounding PL bilayer [21–23]. Also the average polarity around the nitroxide moiety of CSL increases with the increase of the Chol content in DMPC and other PL membranes even beyond the concentration at which the CBD starts to be formed [22,23]. All these indicate that the unfavorable free energy of exposure of the nonpolar part of Chol to water is compensated by the formation of new hydrogen bonds with water, as was indicated in the Introduction.

ASL data show a single value for the NiEDDA accessibility parameters for all Chol contents (Fig. 4B). Very small values of the NiEDDA accessibility parameter indicate that the collision rate between the nitroxide moiety of ASL and NiEDDA in both domains is very low, and confirm that the nitroxide moiety of ASL is located in the hydrocarbon-chain region, close to the membrane center.

After the sample preparation and the first detection of the CBD in DMPC membranes the CBD remains in the samples within hours and even days. Pre-exponential coefficients of SR signals of ASL and CSL in the presence of oxygen and NiEDDA also remain unchanged (within the accuracy of the method) during that time. All these indicate that the system, after reaching equilibrium during tuning spectrometer for EPR measurements and equilibration with a certain partial pressure of oxygen (usually 15 to 30 min), does not change. After perturbation (changing of temperature) membranes go to a new equilibrium, reflected by different EPR spectra and different SR signals. This new equilibrium is reached within a shorter time than the time needed for tuning spectrometer to new conditions. During further measurements, EPR spectra and SR signals do not change. We conclude that measurements were performed for equilibrated systems.

Detection of cholesterol crystals using the DSC

Only monohydrate cholesterol crystals are formed in liposome suspensions prepared using the rapid solvent exchange method—Figure 5 illustrates the first DSC heating scans of Chol crystals formed in suspensions of DMPC liposomes with different Chol content (for Chol/DMPC mixing ratio from 1 to 3). Only for Chol/DMPC molar ratio of 2.25, 2.5, and 3.0, the broad transition peak at ~86°C is observed. This peak indicates conversion of monohydrate Chol crystals to anhydrous Chol crystals [19]. No traces of the peak at 36°C, which indicates the conversion of one crystalline form of anhydrous Chol to another [19,28], were observed for all scans. We can conclude (similarly to Huang et al.[26]) that, when liposome suspension is prepared with the rapid solvent exchange method, only monohydrate Chol crystals are formed at indicated Chol contents. Based on this, we used the excess enthalpy values obtained from the area under the DSC peak at 86°C (Fig. 5) as a quantitative measure of the amount of Chol crystals formed in the suspension.

The DSC was previously used to show formation of Chol crystals in liposome suspensions, but only for samples prepared using the film deposition method [3,4,28,43,44]. In that case, in the first DSC heating scans, two peaks are present at about 36°C and at the region from 76 to 96°C, indicating the conversion of one crystalline form of anhydrous Chol to another (peak at 36°C [28]) and the conversion of monohydrate Chol crystals to anhydrous Chol crystals (peak at 76 to 96°C region [3,28,43]). We also observed two peaks in the first DSC heating scans for Chol/DMPC membranes prepared using the film deposition method (data not shown). To the best of our knowledge, the DSC was never used previously to show the formation of Chol crystals in PL liposome suspensions formed with the rapid solvent exchange method. Instead for these preparations, Chol crystals were detected using X-ray diffraction, a method which also can discriminate anhydrous and monohydrate forms of crystals [26]. We think that the peak observed at 36°C for film deposition method indicates the anhydrous Chol crystals which are formed during demixing of Chol when the lipid mixture passes through the solid state intermediate. Chol trapped in these crystals do not participate in the further liposome formation, giving falsely low estimates of the CST [26]. Thus, for studies on the organization of membranes saturated and oversaturated with Chol, liposomes should be prepared using the rapid solvent exchange method.

CBDs form at cholesterol content lower than the CST

The qualitative explanation of our results is indicated in Figure 1. When the Chol content in the DMPC bilayer increases, the CBDs are formed first at a Chol content significantly lower than the CST. After that, when the Chol content exceeds the CST, Chol crystals form presumably outside the membrane. The former are detected here by EPR spin-labeling methods, the latter by the DSC. CBDs and Chol crystals can be detected only after a significant amount of Chol is accumulated in these Chol structures. Thus, only the extrapolation of the data obtained at different Chol contents to the “zero” amount of Chol in

the CBD or in Chol crystals can give the value of the Chol content at which these structures begin to form.

The pre-exponential factors in the fitting curves of the double-exponential SR signals, in the presence of oxygen (for ASL) and NiEDDA (for CSL), indicate the distribution of Chol analog spin labels between the coexisting CBD and surrounding membrane. If the ASL(CSL)/Chol molar ratio is the same in both domains, pre-exponential coefficients should directly report on the amount of Chol in coexisting domains. If these molar ratios differ, pre-exponential coefficients are still proportional to the amount of Chol in each domain. Thus, the value of the pre-exponential coefficient of the CBD component in SR signal should be proportional to the amount of Chol in the CBD. These values obtained from measurements of ASL and oxygen, and of CSL and NiEDDA are plotted as a function of Chol mixing ratio in Figure 6. For Chol content lower than a Chol/DMPC mixing ratio of 1, no CBD could be detected, indicating that DMPC bilayer is not yet saturated with Chol. Accordingly, with increasing amounts of added Chol, for Chol/DMPC mixing ratios of 1.25, 1.5, and 2.0, the CBD starts to form (Fig. 4). Extrapolation of pre-exponential coefficients presented in Figure 6 indicates that the ~50 mol% is a Chol content at which the pure CBDs begin to form.

In a similar way we analyzed data obtained from the DSC for DMPC membranes containing different amounts of Chol. Here, as a parameter indicating amounts of Chol crystals in the sample, we used the heat of transition value obtained from the area under the DSC peak (Fig. 5). Data presented in Figure 5 clearly shows that Chol crystals in the DMPC suspension can be detected for Chol/DMPC mixing ratios of 2.25, 2.5, and 3.0. Extrapolation of DSC data to the zero value of the heat of transition, as performed in Figure 6, indicates the CST in DMPC membranes is located at the Chol/DMPC mixing ratio of ~2 (66 mol%). This CST value obtained for the DMPC membrane using DSC complements the CST values obtained earlier using X-ray diffraction for different PCs [26]. We should note here that all these membranes were prepared using the rapid solvent exchange method.

The value of the CST expressed in the units of Chol/DMPC ratio is twice as large as a value at which CBDs begin to form within the DMPC bilayer. Thus, at the CST, half of Chol molecules form CBDs and half saturate the surrounding DMPC bilayer. Also, for Chol contents greater than 50 mol%, the presence of the CBD ensure that the surrounding DMPC bilayer is saturated with Chol. It seems that the 66 mol% Chol is the maximal Chol content which can be supported by the DMPC in the form of Chol saturating the DMPC bilayer and Chol forming the CBD.

DISCUSSION

The CBD was detected at high (saturating) Chol content in PC [22], PS [21] and SM [23,24] membranes, as well as in membranes made from the total lipid extracted from animal [35,38,40] and human eye lenses [39]. In all these investigations, the CBD was discriminated only with Chol analog spin labels and not with PL analog spin labels, which indicates that this is a pure Chol domain. EPR spectra of the Chol analog spin labels as well as their orientation in the CBD are typical for the bilayer structure of this domain with the nitroxide moiety of the CSL (replacing the –OH group of Chol) exposed to the water phase and with the nitroxide moiety of ASL (describing location of the isooctyl chain of Chol) located in the hydrophobic core and not accessible to water soluble relaxation agents. The order and mobility of Chol analog spin labels in the CBD are similar to those in the surrounding PL-Chol bilayer confirming that the CBD posses a dynamic structure different from the rigid structure of Chol crystals. These conclusions were also supported by the MD simulations [20].

The properties which can be assigned only to the CBD are oxygen transport parameter and NiEDDA accessibility parameter sensed, respectively, by the ASL and CSL in the CBD. It is clear (Fig. 4) [21–23] that these properties change significantly with the Chol content. For Chol contents just above 50 mol% the oxygen transport and NiEDDA accessibility parameters measured for the CBD are close to those in the surrounding PL-Chol domain. It can be the result of the high exchange rate of Chol molecules between the CBD and surrounding PL-Chol domain and/or high frequency of formation and dissipation of the CBD. Also, other properties sensed by ASL and CSL which cannot be resolved between CBD and PL-Chol domain (properties that depend on the order and motion of these spin labels) change significantly with the increase of Chol content above that at which formation of the CBD started [22,24]. Thus, in the range of Chol content between 50 and 66 mol%, not only the changes of the relative amounts of CBDs and PC-Chol domain take place, but also properties of the CBD are not constant characteristics of this domain. This suggests that for Chol contents just above 50 mol% the size of the individual domain is rather small and increases with the increased Chol content. This also suggests that the size of the interface is large enough relative to the size of the domain, and its contribution to the properties of Chol molecules forming the CBD cannot be neglected. Additionally, properties of Chol molecules forming the CBD depend on the exchange rate of Chol between the CBD and the PL-Chol domain, which, taking into account high dynamics of the CBD, can be considerable. Based on the discussion regarding “domains and phases” in [45,46] we conclude that the CBD is not forming a separate phase but is represented by rather small pure Chol domains surrounded by PL bilayer saturated with Chol.

Results obtained for membranes made of different PLs indicate that the bulk membrane properties of the PL-Chol bilayer do not change for Chol contents exceeding that at which the CBD starts to be formed (at which the PL-Chol domain become saturated with Chol) [23,24,35,47]. Bulk membrane properties include detailed profiles of the order parameter, fluidity, oxygen transport parameter and hydrophobicity obtained with PL analog spin labels without contamination from the CBD [35]. At 50 mol% Chol DMPC bilayer forms the liquid-ordered phase saturated with Chol. Thus, we can conclude that the formation of the CBD does not affect properties of that liquid-ordered phase.

We would like to combine our results, which includes regions of Chol contents below and above the CST in DMPC membranes (located at 66 mol% Chol), with the established phase diagram for Chol/DMPC membranes [29]. The CBDs, organized as dynamic pure Chol bilayers, form Chol patches within the DMPC-Chol bilayer saturated with Chol. However, properties of the surrounding DMPC-Chol bilayer do not change after saturation with Chol (after formation of the CBD). Thus, the region of the phase diagram for Chol contents between 50 and 66 mol% might be described as a structured one-phase region [48] and not as a two-phase coexisting region. In the terminology of Simons and Vaz [49] such a region can be called a dispersed phase. This structured liquid-ordered phase of the DMPC membrane exists above 50 mol% Chol. At 66 mol% Chol, monohydrate Chol crystals start to form. They possess rigid three-dimensional structure formed from multiple layers of Chol. This pseudo bilayer structure is vastly different from the dynamic structure of Chol bilayers in the CBD. This discussion is summarized in Figure 7 where the phase boundary located at 66 mol% Chol (at CST) separates the structured one-phase region (liquid-ordered phase of DMPC with CBDs) from the two-phase region where the structured liquid-ordered phase of DMPC coexists with Chol crystals. In that phase diagram we indicated the region of Chol contents where the structured liquid-ordered phase of the DMPC membrane is formed.

CONCLUSIONS

The major result of this research, which was possible because of the use of the rapid solvent exchange method for liposome preparation, is that the formation of CBDs precedes formation of Chol crystals (Fig. 7). These domains are supported by the surrounding DMPC membrane saturated with Chol. Most likely these domains form precursors for Chol crystals. As we indicated above, the size of the individual domain is rather small. When, after addition of Chol the size of the domain increases above the limited size which cannot be further supported by the surrounding PL bilayer, CBD collapses from the two-dimensional structure of the domain to the three-dimensional structure of the monohydrate Chol crystal. It is assumed that, after formation, Chol crystals are located outside the PL bilayer.

Acknowledgments

This work was supported by grants EY015526, EB002052, and EB001980 of the National Institutes of Health. We thank Dr. Jeffrey T. Buboltz at University of Wisconsin-Platteville for his help in building the rapid solvent exchange device.

References

1. Wachtel EJ, Borochov N, Bach D. The Effect of Protons or Calcium Ions on the Phase Behavior of Phosphatidylserine-Cholesterol Mixtures. Biochim Biophys Acta. 1991; 1066:63–69. [PubMed: 1648395]
2. Borochov N, Wachtel EJ, Bach D. Phase Behavior of Mixtures of Cholesterol and Saturated Phosphatidylglycerols. Chem Phys Lipids. 1995; 76:85–92. [PubMed: 7788803]
3. Epand RM. Cholesterol in Bilayers of Sphingomyelin or Dihydrosphingomyelin at Concentrations Found in Ocular Lens Membranes. Biophys J. 2003; 84:3102–3110. [PubMed: 12719240]
4. Epand RM, Hughes DW, Sayer BG, Borochov N, Bach D, Wachtel E. Novel Properties of Cholesterol-Dioleoylphosphatidylcholine Mixtures. Biochim Biophys Acta. 2003; 1616:196–208. [PubMed: 14561477]
5. Mason R, Tulenko TN, Jacob RF. Direct Evidence for Cholesterol Crystalline Domains in Biological Membranes: Role in Human Pathobiology. Biochim Biophys Acta. 2003; 1610:198–207. [PubMed: 12648774]
6. Cheetham JJ, Wachtel E, Bach D, Epand RM. Role of the Stereochemistry of the Hydroxyl Group of Cholesterol and the Formation of Nonbilayer Structures in Phosphatidylethanolamines. Biochemistry. 1989; 28:8928–8934. [PubMed: 2557911]
7. Tulenko TN, Chen M, Mason PE, Mason RP. Physical Effects of Cholesterol on Arterial Smooth Muscle Membranes: Evidence of Immiscible Cholesterol Domains and Alterations in Bilayer Width During Atherogenesis. J Lipid Res. 1998; 39:947–956. [PubMed: 9610760]
8. Jacob RF, Cenedella RJ, Mason RP. Direct Evidence for Immiscible Cholesterol Domains in Human Ocular Lens Fiber Cell Plasma Membranes. J Biol Chem. 1999; 274:31613–31618. [PubMed: 10531368]
9. Guo W, Hamilton JA. 13C MAS NMR Studies of Crystalline Cholesterol and Lipid Mixtures Modeling Atherosclerotic Plaques. Biophys J. 1996; 71:2857–2868. [PubMed: 8913623]
10. Bach D, Wachtel E. Phospholipid/Cholesterol Model Membranes: Formation of Cholesterol Crystallites. Biochim Biophys Acta. 2003; 1610:187–197. [PubMed: 12648773]
11. Mason RP, Jacob RF. Membrane Microdomains and Vascular Biology: Emerging Role in Atherogenesis. Circulation. 2003; 107:2270–2273. [PubMed: 12732593]
12. Ziblat R, Leiserowitz L, Addadi L. Crystalline Domain Structure and Cholesterol Crystal Nucleation in Single Hydrated DPPC:Cholesterol:POPC Bilayers. J Am Chem Soc. 2010; 132:9920–9927. [PubMed: 20586463]
13. Ziblat R, Fargion I, Leiserowitz L, Addadi L. Spontaneous Formation of Two-Dimensional and Three-Dimensional Cholesterol Crystals in Single Hydrated Lipid Bilayers. Biophys J. 2012; 103:255–264. [PubMed: 22853903]

14. Ziblat R, Leiserowitz L, Addadi L. Crystalline Lipid Domains: Characterization by X-Ray Diffraction and Their Relation to Biology. Angew Chem. 2011; 50:3620–3629. [PubMed: 21472900]
15. Borchman D, Yappert MC. Lipids and the Ocular Lens. J Lipid Res. 2010; 51:2473–2488. [PubMed: 20407021]
16. Troup GM, Tulenko TN, Lee SP, Wrenn SP. Estimating the Size of Laterally Phase Separated Cholesterol Domains in Model Membranes with Forster Resonance Energy Transfer: A Simulation Study. Coll Surf B: Biointer. 2004; 33:57–65.
17. Jacob RF, Mason RP. Lipid Peroxidation Induces Cholesterol Domain Formation in Model Membranes. J Biol Chem. 2005; 280:39380–39387. [PubMed: 16195227]
18. Mason RP, Walter MF, Day CA, Jacob RF. Active Metabolite of Atorvastatin Inhibits Membrane Cholesterol Domain Formation by an Antioxidant Mechanism. J Biol Chem. 2006; 281:9337–9345. [PubMed: 16464853]
19. Loomis CR, Shipley GG, Small DM. The Phase Behavior of Hydrated Cholesterol. J Lipid Res. 1979; 20:525–535. [PubMed: 458269]
20. Plesnar E, Subczynski WK, Pasenkiewicz-Gierula M. Comparative Computer Simulation Study of Cholesterol in Hydrated Unary and Binary Lipid Bilayers and in an Anhydrous Crystal. J Phys Chem B. 201310.1021/jp402839r
21. Raguz M, Mainali L, Widomska J, Subczynski WK. The Immiscible Cholesterol Bilayer Domain Exists as an Integral Part of Phospholipid Bilayer Membranes. Biochim Biophys Acta. 2011; 1808:1072–1080. [PubMed: 21192917]
22. Raguz M, Mainali L, Widomska J, Subczynski WK. Using Spin-Label Electron Paramagnetic Resonance (EPR) to Discriminate and Characterize the Cholesterol Bilayer Domain. Chem Phys Lipids. 2011; 164:819–829. [PubMed: 21855534]
23. Mainali L, Raguz M, Subczynski WK. Phase-Separation and Domain-Formation in Cholesterol-Sphingomyelin Mixture: Pulse-EPR Oxygen Probing. Biophys J. 2011; 101:837–846. [PubMed: 21843474]
24. Mainali L, Raguz M, Subczynski WK. Phases and Domains in Sphingomyelin-Cholesterol Membranes: Structure and Properties Using EPR Spin-Labeling Methods. Eur Biophys J. 2012; 41:147–159. [PubMed: 22033879]
25. Plesnar E, Subczynski WK, Pasenkiewicz-Gierula M. Saturation with Cholesterol Increases Vertical Order and Smoothes the Surface of the Phosphatidylcholine Bilayer: A Molecular Simulation Study. Biochim Biophys Acta. 2012; 1818:520–529. [PubMed: 22062420]
26. Huang J, Buboltz JT, Feigenson GW. Maximum Solubility of Cholesterol in Phosphatidylcholine and Phosphatidylethanolamine Bilayers. Biochim Biophys Acta. 1999; 1417:89–100. [PubMed: 10076038]
27. Buboltz JT, Feigenson GW. A Novel Strategy for the Preparation of Liposomes: Rapid Solvent Exchange. Biochim Biophys Acta. 1999; 1417:232–245. [PubMed: 10082799]
28. Benatti CR, Lamy MT, Epand RM. Cationic Amphiphiles and the Solubilization of Cholesterol Crystallites in Membrane Bilayers. Biochim Biophys Acta. 2008; 1778:844–853. [PubMed: 18201547]
29. Almeida PF, Vaz WL, Thompson TE. Lateral Diffusion in the Liquid Phases of Dimyristoylphosphatidylcholine/Cholesterol Lipid Bilayers: A Free Volume Analysis. Biochemistry. 1992; 31:6739–6747. [PubMed: 1637810]
30. Buboltz JT. A More Efficient Device for Preparing Model-Membrane Liposomes by the Rapid Solvent Exchange Method. Rev Sci Instrum. 2009; 80:124301. [PubMed: 20059155]
31. Yin JJ, Subczynski WK. Effects of Lutein and Cholesterol on Alkyl Chain Bending in Lipid Bilayers: A Pulse Electron Spin Resonance Spin Labeling Study. Biophys J. 1996; 71:832–839. [PubMed: 8842221]
32. Hyde, JS.; Subczynski, WK. Biological Magnetic Resonance. Berliner, LJ.; Reuben, J., editors. Vol. 8. Plenum Press; New York: 1989. p. 399-425.
33. Kusumi A, Subczynski WK, Hyde JS. Oxygen Transport Parameter in Membranes as Deduced by Saturation Recovery Measurements of Spin-Lattice Relaxation Times of Spin Labels. Proc Natl Acad Sci U S A. 1982; 79:1854–1858. [PubMed: 6952236]

34. Subczynski WK, Felix CC, Klug CS, Hyde JS. Concentration by Centrifugation for Gas Exchange EPR Oximetry Measurements with Loop-Gap Resonators. J Magn Reson. 2005; 176:244–248. [PubMed: 16040261]
35. Raguz M, Widomska J, Dillon J, Gaillard ER, Subczynski WK. Characterization of Lipid Domains in Reconstituted Porcine Lens Membranes Using EPR Spin-Labeling Approaches. Biochim Biophys Acta. 2008; 1778:1079–1090. [PubMed: 18298944]
36. Subczynski, WK.; Widomska, J.; Wisniewska, A.; Kusumi, A. Methods in Molecular Biology, Lipid Rafts. McIntosh, TJ., editor. Vol. 398. Humana Press; Totowa: 2007. p. 143-157.
37. Subczynski WK, Wisniewska A, Hyde JS, Kusumi A. Three-Dimensional Dynamic Structure of the Liquid-Ordered Domain as Examined by a Pulse-EPR Oxygen Probing. Biophys J. 2007; 92:1573–1584. [PubMed: 17142270]
38. Raguz M, Widomska J, Dillon J, Gaillard ER, Subczynski WK. Physical Properties of the Lipid Bilayer Membrane Made of Cortical and Nuclear Bovine Lens Lipids: EPR Spin-Labeling Studies. Biochim Biophys Acta. 2009; 1788:2380–2388. [PubMed: 19761756]
39. Mainali L, Raguz M, O'Brien WJ, Subczynski WK. Properties of Membranes Derived from the Total Lipids Extracted from the Human Lens Cortex and Nucleus. Biochim Biophys Acta. 2013; 1828:1432–1440. [PubMed: 23438364]
40. Mainali L, Raguz M, O'Brien WJ, Subczynski WK. Properties of Fiber Cell Plasma Membranes Isolated from the Cortex and Nucleus of the Porcine Eye Lens. Exp Eye Res. 2012; 97:117–129. [PubMed: 22326289]
41. Huang J, Feigenson GW. A Microscopic Interaction Model of Maximum Solubility of Cholesterol in Lipid Bilayers. Biophys J. 1999; 76:2142–2157. [PubMed: 10096908]
42. Huang J. Exploration of Molecular Interactions in Cholesterol Superlattices: Effect of Multibody Interactions. Biophys J. 2002; 83:1014–1025. [PubMed: 12124283]
43. Epand RM, Bach D, Epand RF, Borochov N, Wachtel E. A New High-Temperature Transition of Crystalline Cholesterol in Mixtures with Phosphatidylserine. Biophys J. 2001; 81:1511–1520. [PubMed: 11509364]
44. Epand RM, Epand RF, Hughes DW, Sayer BG, Borochov N, Bach D, Wachtel E. Phosphatidylcholine Structure Determines Cholesterol Solubility and Lipid Polymorphism. Chem Phys Lipids. 2005; 135:39–53. [PubMed: 15854624]
45. Almeida PF, Pokorny A, Hinderliter A. Thermodynamics of Membrane Domains. Biochim Biophys Acta. 2005; 1720:1–13. [PubMed: 16472555]
46. Almeida PF. Thermodynamics of Lipid Interactions in Complex Bilayers. Biochim Biophys Acta. 2009; 1788:72–85. [PubMed: 18775410]
47. Subczynski WK, Raguz M, Widomska J, Mainali L, Konovalov A. Functions of Cholesterol and the Cholesterol Bilayer Domain Specific to the Fiber-Cell Plasma Membrane of the Eye Lens. J Membr Biol. 2012; 245:51–68. [PubMed: 22207480]
48. Heberle FA, Feigenson GW. Phase Separation in Lipid Membranes. Cold Spring Harb Perspect Biol. 2011; 3:1–13.
49. Simons K, Vaz WL. Model Systems, Lipid Rafts, and Cell Membranes. Annu Rev Biophys Biomol Struct. 2004; 33:269–295. [PubMed: 15139814]

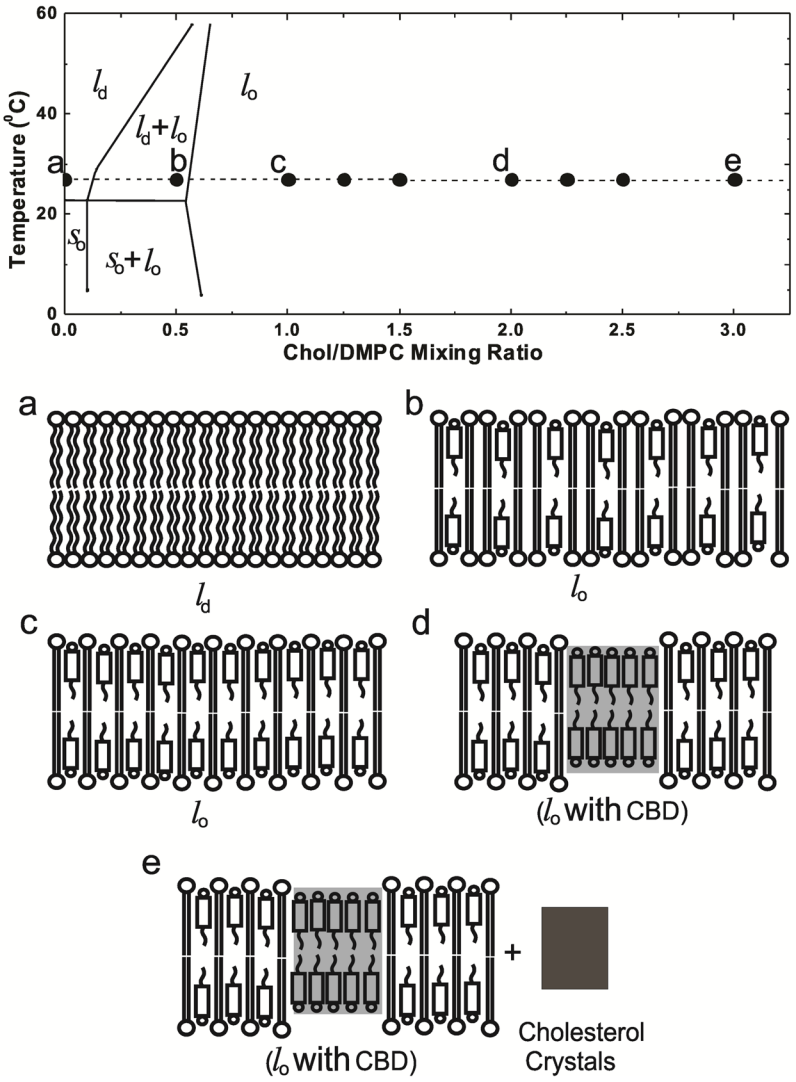

Figure 1.

Experiments were performed for cholesterol contents extending beyond the established phase diagram [29], included in the figure. The broken line and solid circles indicate the temperature and Chol/DMPC mixing ratios at which measurements were performed. Schematic drawings of purported membrane structures (including phases, domains, and crystals) formed at different Chol/DMPC mixing ratios [(a) 0, (b) 1/2; (c) 1/1; (d) 2/1, and (e) 3/1] are presented. l_d – liquid disordered phase, l_o – liquid ordered phase, s_o – solid ordered phase, and CBD – cholesterol bilayer domain.

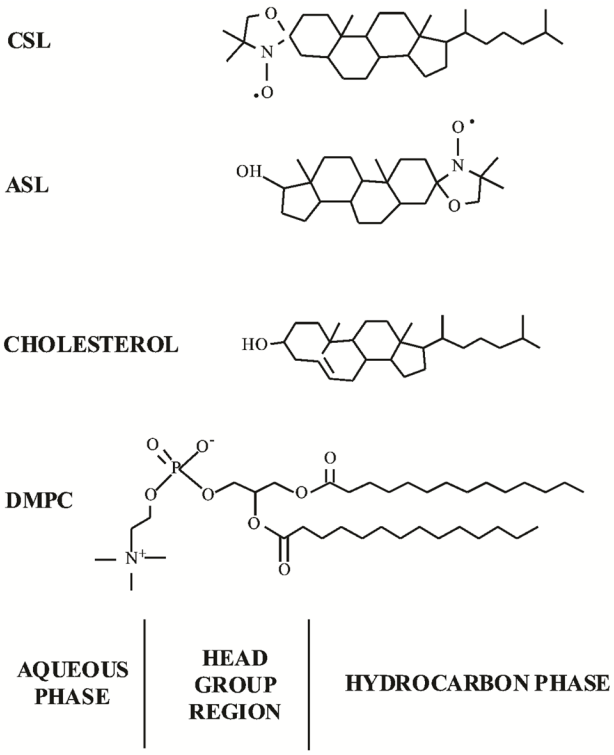

Figure 2.
Chemical structures of cholesterol analog spin labels used in this work: ASL and CSL. Chemical structures of DMPC and cholesterol are also included to indicate approximate locations of these molecules across the PL bilayer membrane.

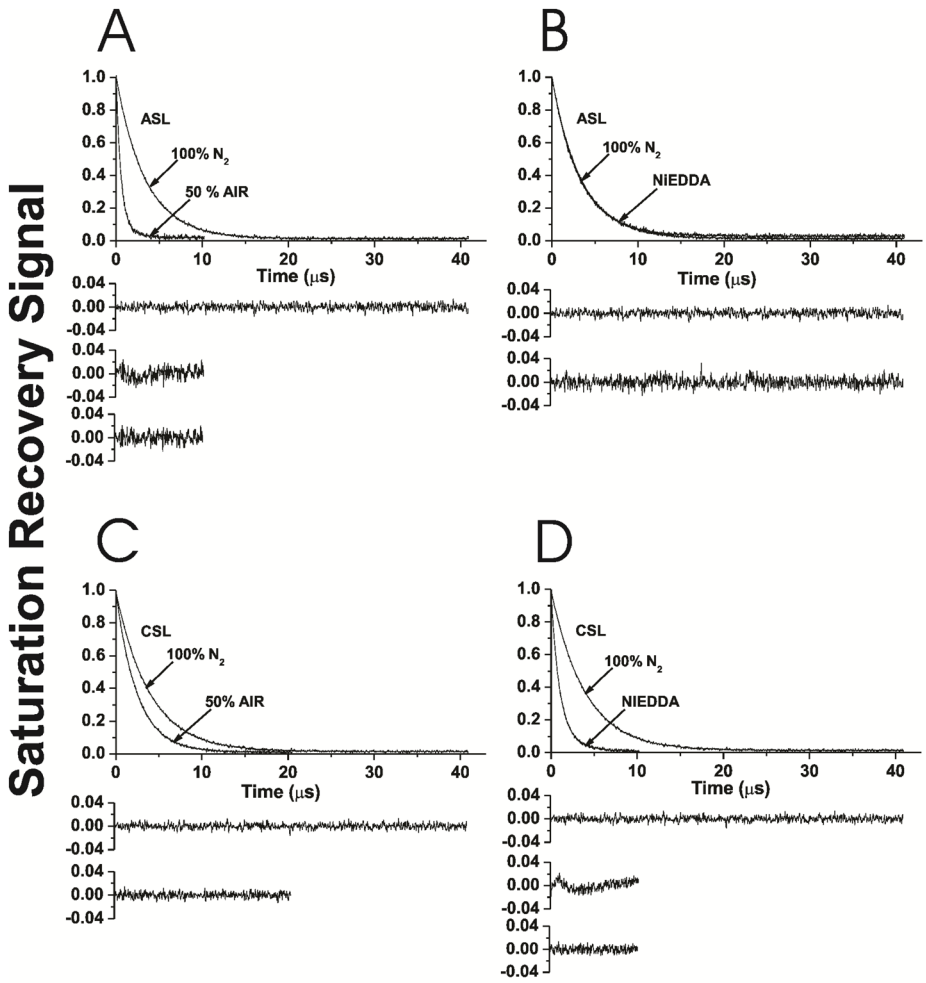

Figure 3.

Representative SR signals with fitted curves and residuals (the experimental signal minus the fitted curve) for ASL (A, B) and CSL (C, D) in Chol/DMPC membranes with a Chol/DMPC mixing ratio of 1.5. Signals were recorded at 27°C for samples equilibrated with 100% nitrogen (A, B, C, D); with a gas mixture of 50% air and 50% nitrogen (A, C); and in the presence of NiEDDA (B, D). For simpler comparison with other data, the SR signals for samples equilibrated with 100% nitrogen were duplicated in (A) and (B) for ASL, and in (C) and (D) for CSL. SR signals were satisfactorily fitted to a single-exponential function in the absence of molecular oxygen with time constants of 3.30 ± 0.01 μs (A), 3.30 ± 0.01 μs (B), 3.96 ± 0.01 μs (C), and 3.96 ± 0.01 μs (D) (the upper residuals in A, B, C, and D are for a single-exponential fit). The SR signal in the presence of molecular oxygen can be fitted satisfactorily with a single-exponential function only for CSL with a time constant of 2.47 ± 0.01 μs (C) (lower residual in C is for a single-exponential fit), and with double-exponential curves for ASL with time constants of 1.39 ± 0.03 μs and 0.66 ± 0.01 μs (A) (middle residual in A is for single- and lower residual for double-exponential fits). The SR signal in the presence of NiEDDA can be fitted satisfactorily with a single-exponential function only for ASL with a time constant of 3.26 ± 0.01 μs (B) (lower residual in B is for single-exponential fit) and with double-exponential curves for CSL with time constants of 1.92 ± 0.05 μs and 0.99 ± 0.01 μs (D) (middle residual in D is for single- and lower residual for double-exponential fits). The uncertainties in the measurements of decay times (standard

deviations given by the fitting program) from the fits of individual SR signals to the single- or double-exponential curves are indicated.

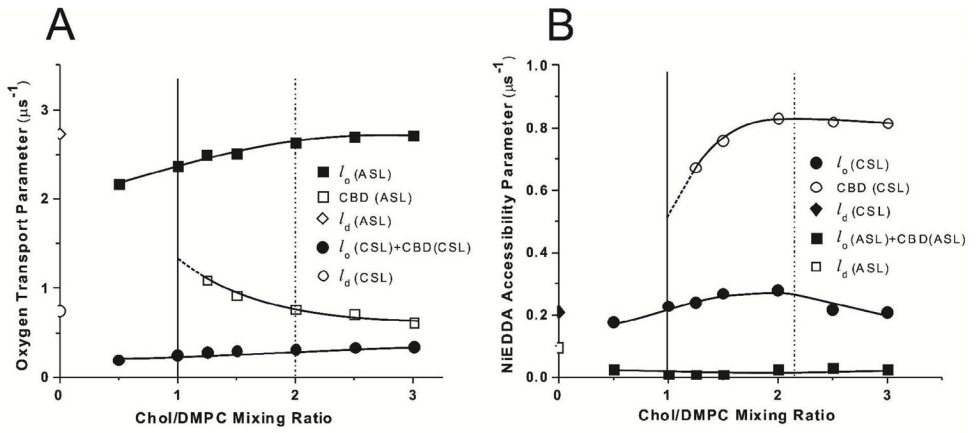

Figure 4.

The oxygen transport parameter, $W(x)$, calculated based on Eqs. (1), (3) and (4) (A) and NiEDDA accessibility parameter, $P(x)$, calculated based on Eqs. (2), (5) and (6) (B) for ASL and CSL in Chol/DMPC membranes plotted as a function of the Chol/DMPC mixing ratio. Values of these parameters in coexisting phases (domains) are indicated. Vertical solid and broken lines indicate the upper limit of the cholesterol concentration that can be accommodated within the liquid-ordered phase of the DMPC membrane and the CST in the DMPC membrane.

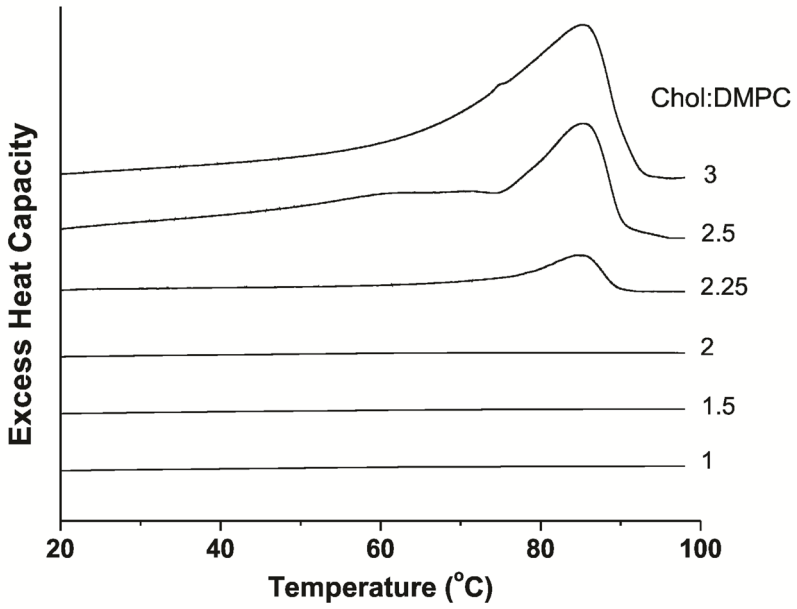

Figure 5.
First DSC heating scans of Chol/DMPC dispersions with different cholesterol contents.

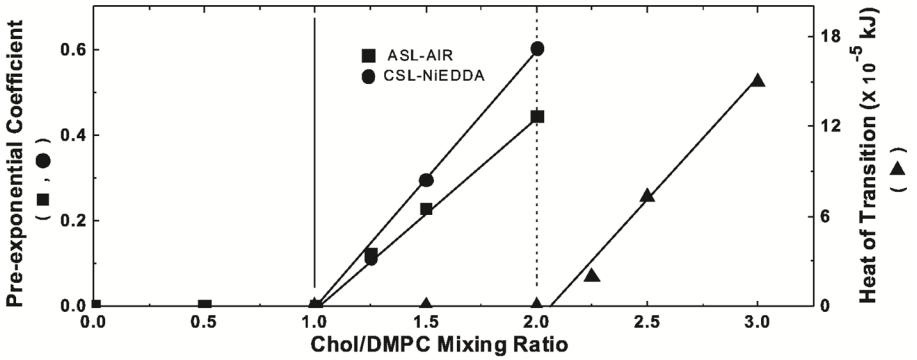

Figure 6.

Plot of the pre-exponential coefficient of the CBD component in SR signal obtained from measurements with ASL (■) and CSL (●) and the excess enthalpy value (area under the peak at ~86°C plotted as a function of cholesterol content (Chol/DMPC molar ratio) (▲) in DMPC suspension. Pre-exponential coefficients were measured for samples equilibrated with 50% air (ASL) and in the presence of 20 mM NiEDDA (CSL). Vertical solid and broken lines indicate the upper limit of the cholesterol concentration that can be accommodated within the liquid-ordered phase of the DMPC membrane and the CST in the DMPC membrane.

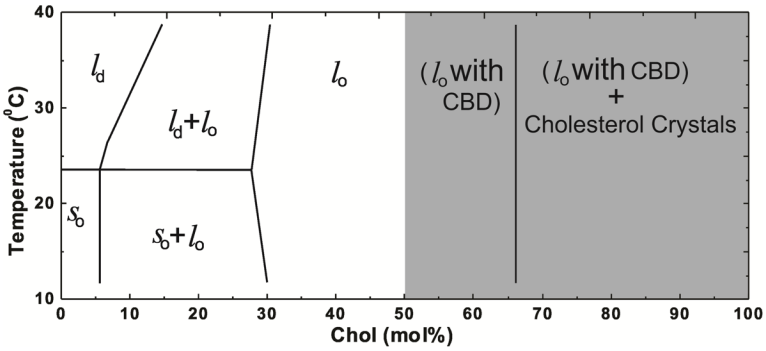

Figure 7.

Extension of the established phase diagram for Chol/DMPC mixtures [29] to the region, indicated by the shaded area, where CBDs are detected, forming the structured liquid-ordered phase of DMPC membranes. The CST (located at 66 mol% Chol for DMPC membranes prepared using the rapid solvent exchange method) is indicated. This phase boundary separates the structured one-phase region (liquid-ordered phase of DMPC with CBDs) from the two-phase region where the structured liquid-ordered phase of DMPC coexists with Chol crystals.